The ATLAS Pixel Detector

Beniamino Di Girolamo[*]
CERN, Geneve
E-mail: Beniamino.Di.Girolamo@cern.ch
on behalf of the ATLAS Collaboration

This paper presents an overview of the ATLAS Pixel Detector from the detector description to few examples of the performance while illustrating the work invested to achieve a high precision calibration. The strategy for detecting the effects of radiation damage is presented. The final part of the paper is then dedicated to the current data taking status.

[*]Speaker.

1. Introduction

The ATLAS detector [1] is one of the general purpose experiments installed at the Large Hadron Collider (LHC) at CERN, and the largest high energy apparatus ever built. It is designed to study processes at the TeV scale, search for the Higgs boson and for physics beyond the Standard Model as well as to make precision measurements of the Standard Model.

The detector is subdivided in three main systems:

- an Inner Detector operating inside a solenoidal magnet at 2 T and described with some details later;

- a barrel and end-cap hybrid calorimetry system based on LAr technology and different types of absorber materials for the central electromagnetic calorimeter and end-cap electromagnetic and hadronic calorimeters; the central barrel hadronic calorimeter is instead based on iron-scintillator technology;

- a Muon Spectrometer in a toroidal field of 4 T produced by a large air-core toroidal 3-magnets system, with a variety of gas chamber technologies.

The ATLAS Inner Detector includes three different sub-detectors: an outer straw-tubes based tracker with particle identification capabilities based on transition radiation effects (Transition Radiation Tracker, TRT), a silicon strip detector (SemiConductor Tracker, SCT) and finally the innermost silicon pixel detector (Pixel Detector).
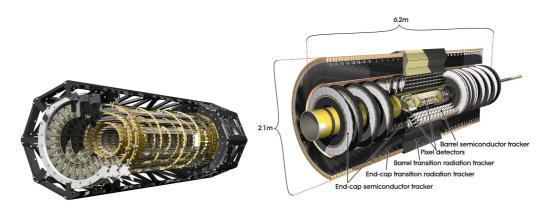

Figure 1: The ATLAS Pixel Detector (left) and the full Inner Detector (right)

The Inner Detector is 6.2 m long and has a diameter of 2.1 m (fig. 1). It has an acceptance in the range $|\eta| < 2.5$ ($|\eta| < 2$ for TRT). The Inner Detector has been designed to achieve a momentum resolution of $\sigma(p_T)/p_T = 0.05\% \, p_T \, [\text{GeV}/c] \oplus 1\%$ and an impact parameter resolution of $\sigma(d_0) = 10 \, \mu\text{m} \oplus 140 \, \mu\text{m}/p_T \, [\text{GeV}/c]$, in the range $0.25 < |\eta| < 0.5$,

2. The ATLAS Pixel Detector

2.1 Properties and requirements

The Pixel Detector is built out of 1744 identical modules assembled in three barrel layers and three disks, on each side of the barrel (fig. 1). Each of the six disks is made of eight sectors with six modules each (288 modules in total). Each barrel layer is built with modules on local supports (staves) and on each stave there are thirteen modules (1456 modules in total). The total number of readout channels is approximately 80 millions [2].

The innermost layer is placed at only 50.5 mm from the interaction point, with small clearance from the beam pipe. These extreme conditions imposed a requirement for a radiation tolerance up to 500 kGy for a fluence of 10^{15} 1 MeV n_{eq} cm^{-2} and the adoption of an evaporative C_3F_8-based cooling integrated in the modules supports to keep the modules' temperature below 0 °C and remove the heat generated by the electronics. The detector is operated at a coolant temperature of -20 °C (corresponding in average to -13 °C on detector) since Summer 2009; the cooling system is able to operate down to a coolant temperature of -30 °C and this temperature setting will be exploited only later in the detector life when the radiation damage effects will be more important.

The detector has been designed, built and tested to achieve a position resolution in $r - \phi$ of less than 15 μm, three track points for $|\eta| < 2.5$, a time resolution of less than 25 ns and a hit detection efficiency higher than 97 %.
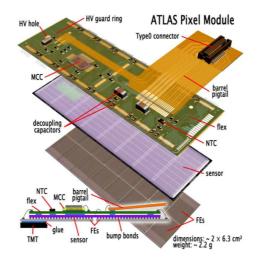

Figure 2: The ATLAS Pixel Module

A 4th innermost layer, to be placed at about 30 mm from the interaction point, is being built to be installed in 2013 [3].

2.2 The ATLAS Pixel Module

The Pixel modules (fig. 2) are built using 250 μm thick n-on-n Si sensors with 47232 pixels and a pixel size of 50 μm × 400 μm, except for a fraction of long pixels with a size of 50 μm × 600 μm; these latter pixels are located in the inter-chip regions. Each module is operated at a bias voltage of 150-600 V (150 V are used for the present, not yet irradiated, detector) and read out using 16

Front-End chips (FE-I3 ASICs [4]) with 2880 readout channels each. The 16 chips read out in total 46080 channels, but all 47232 pixels are readout, as pixels in the inter-chip regions are ganged together to be read out.

The FE-I3 front-end chip allows for pulse height measurements by means of the Time-over-Threshold determination. Zero-suppression is performed on chip. An event building chip, the Module Controller Chip (MCC) [5], collects the data from the 16 readout chips. The data is then converted into optical signals and sent via optical fibres to the off-detector electronics with a data transfer speed of 40 to 160 MHz, adjusted accordingly to the expected occupancy. The MCC also provides clock and control signals to the individual front-end chips.

3. The Pixel Detector Commissioning and Calibration

The Pixel Detector installation was completed in Spring 2008. The period between August and December 2008 was dedicated to functionality checks, calibrations and finally cosmic ray data taking.

The first calibration campaign in 2008 allowed to establish a very robust baseline configuration with a setting of the threshold at 4000 e for the full detector with minimal dispersion. The Pixel Detector can only be switched on with stable conditions of the LHC beams (known as "Stable Beams") and this condition was satisfied for the first time in November 2009 with a single 450 GeV pilot beam and finally with collisions at $\sqrt{s} = 900$ GeV for the first time on December 6th, 2009. At that time the threshold setting had already been further improved and set to the lower value of 3500 e, that is the current configuration. The results from the LHC collisions will be discussed in a next section, after a description of the very important aspect of getting the detector precisely calibrated.

3.1 The calibration procedures and results

The Pixel Detector has a large set of possible calibration parameters. The first important step in calibrating the detector consists in the setting up the optical communication between the detector modules and the off-detector readout electronics.

A large set of parameters of the front-end electronics can be calibrated and tuned to achieve a small dispersion of those parameters, across all channels on a front-end chip, on a complete module and finally on the complete detector. An internal calibration circuitry in each front-end chip allows to inject test charges into the pre-amplifier input, simulating in this way a charge deposition in the sensor, with a predefined value of charge and timing.

The front-end chip contains a discriminator stage per pixel to allow for an efficient noise rejection via the setting of a threshold, determined from the fitting of the noise integral function. The threshold can be set via a 7-bit DAC that allows an adjustment for each pixel. The DAC settings are determined via calibration scans. The subsequent tuning procedure allows to obtain an homogeneous threshold setting among different pixels, eliminating response differences, within the achievable threshold dispersion.

The results obtained are quite good, as can be seen in figure 3. It shows the results for the 3500 e setting with a dispersion of 40 e and a fraction of masked pixels around 0.1 %. An effort to prepare a configuration with a threshold set at 3000 e is ongoing with lower priority as the

current setting suits the tracking and cluster size needs. The aim of preparing a lower threshold configuration is mainly justified for future operations with a radiation damaged detector in few years from now.

The noise has been measured to be approximately 170 e for most pixels, being slightly higher (~ 300 e) for longer and ganged pixels. The threshold-to-noise ratio is ~ 25 for the majority of the pixels in the detector (figure 3). The noise occupancy after masking noisy pixels is at the level of 10^{-9} hits per pixel per event.
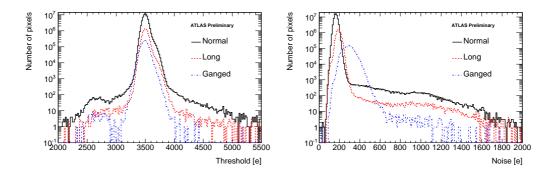

Figure 3: The threshold (left) and noise (right) distributions per pixel for the 3500 e threshold setting. Both plots are in log scale to enhance the small contributions of the tails.

When a charge deposited in the sensor is above the discriminator threshold, the front-end electronics stores the Time-over-Threshold (ToT) quantity, i.e. the time during which the pre-amplifier output is above threshold. By design the ToT has a nearly linear dependence on the amplitude of the pre-amplifier output and therefore on the charge released in the sensor. A 3-bit DAC allows to adjust the pre-amplifier feedback current and therefore the ToT value and its behavior. The ToT response is calibrated and tuned, via charge injections, to have a homogeneous response of approximately 20000 e, corresponding to the most probable value for the charge deposited by one m.i.p. in the silicon sensor. A ToT target value of 30, in bunch crossing (BC) units (1 BC = 25 ns), is obtained.
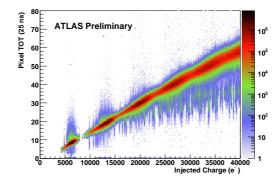

Figure 4: The ToT vs. injected charge calibration plot

Figure 4 shows the calibration curve ToT vs. injected charge .

4. Detector performance with optimal calibration

4.1 Exploitation of the charge measurement

The measurement of the deposited charge, obtained with the calibration of the ToT, allows several improvements for the detector performance. The impact on the position resolution is clearly visible in figure 5 where the improvement is obtained by weighting properly the pixel hit in a cluster with a charge sharing algorithm and define the track position with enhanced precision with respect to a purely digital approach (center of cluster algorithm mentioned in the plot). The Landau curve confirms the ToT calibration with a most probable value of ~ 20000 e in good agreement with the simulation for tracks with $p_T > 100$ MeV.
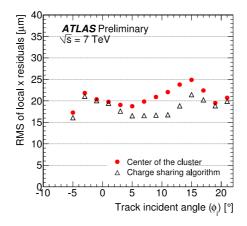

Figure 5: The plot illustrates the improvement in position resolution in the precision direction in $r\phi$ (local x) vs. the track incident angle.

It is also worth mentioning that the hit-to-track association efficiency is at the level of 99 % for nearly all detector parts with a lower efficiency for one of the end-cap disks due to few defects on individual modules (figure 6).
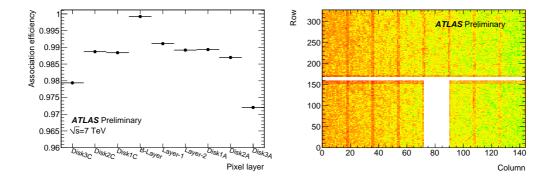

Figure 6: The track association efficiency and an example of defects on individual modules that cause a lower efficiency for one of the end-cap disks (Disk3A).

Another important application of the ToT information is the determination of the track dE/dx obtained by selection of the proper clusters to ensure a full charge collection. The selection eliminates clusters at the edge of modules where the charge can only be partially collected. As a result of this selection, 91 % of the track clusters are retained. The plot in figure 7 shows that there is a clear identification for π, K, protons and, on the positive particle side, for deuterons. The track dE/dx resolution is ~ 12 %.
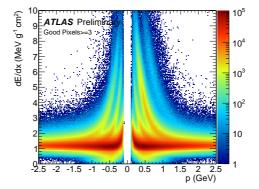

Figure 7: The track dE/dx is calculated starting from the charge collected in the pixel clusters associated to the track itself.

4.2 The Lorentz angle

The Pixel Detector operates in a solenoidal field of 2 T, therefore the Lorentz anagle needs to be determined with good accuracy, by measuring the mean cluster size as a function of the track incident angle. The measured value of $\theta_L = (211.3 \pm 1.6)$ mrad is close to the expected value of 225 mrad (fig. 8). In addition it is possible to use the Pixel Detector as a powerful thermometer to measure the behavior of the Lorentz angle with the temperature, i.e. the temperature dependence of the electron mobility. The measured value of $d\alpha/dT = (-0.78 \pm 0.18)$ mrad/K is in agreement with the theoretical expectation of -0.74 mrad/K [6].
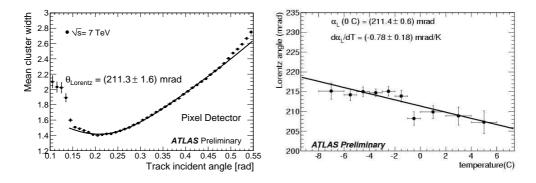

Figure 8: The Lorentz angle plot (left) and the Lorentz angle dependence on the operating temperature (right)

4.3 The timing performance and the reduction of the "overdrive"

The adjustment of the module by module timing via several optimization, from the cable length adjustment to the final timing scans, allowed to reach a very good level of homogeneity and stability.

After all timing adjustment a module-to-module dispersion of $7 \cdot 10^{-3}$ BC, corresponding to 0.17 ns, has been achieved for the setting of a readout window of 1 BC. The module timing histogram in figure 9 (left plot) is obtained from the measurement of the average detection time for large charges. The stability of the measurement is monitored looking at the stability of the delay setting in the optical link tuning that is a measure of the position of the optical link operating point. The timing is constantly verified with calibrations to ensure that the signal is always well contained inside a single bunch crossing wide readout window.
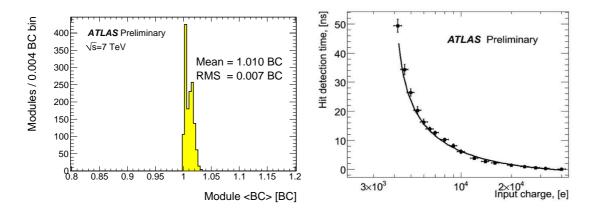

Figure 9: The module synchronization can be assessed by checking the average bunch crossing detected for high charge (>15 000 e) single-pixel clusters. The bin width is 0.004 BC = 0.1 ns. On the right: the time walk profile indicating the variation of the hit detection time as a function of the input charge.

The high precision of the time measurement allows for a correction of the time-walk effect, typical of a threshold based system. The hits with a lower charge suffer of time-walk that can lead to the association of the hit to a wrong bunch crossing. This effect leads to the definition of an intime-threshold as the value of the threshold such that all hits are associated to the correct bunch crossing. As can be seen in figure 9 (right plot) the hit detection time has a rapid variation with the charge of a given hit. This effect makes the effective in-time threshold to be higher (4800 e) than the one set (3500 e). The difference between the in-time threshold and the threshold is often called "overdrive".

The Pixel Front-End chip (FEI3) has a mechanism associated with a digital threshold, that allows to compensate for the time-walk effects by copying the late hits information to the previous bunch crossing, recovering in this way what would be otherwise lost. The digital threshold is set as a minimal value in terms of ToT and in the specific case a value of 7 BC as been found as the optimal setting.

That allows to recover the hits with a lower charge that would otherwise be lost because of their late arrival. In this way the in-time threshold value is reduced to ~ 3700 e with a reduction

of the threshold dispersion from ~ 200 to ~ 100 e. The "overdrive" is therefore reduced to only ~ 200 e w.r.t. the 1300 e value obtained before (fig. 10).
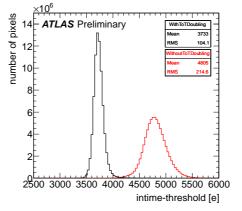

Figure 10: The plot shows how the hit-doubling mechanism illustrated in the text allows to have a reduction of the intime-threshold value from 4800 e to 3700 e, i.e. only 200 e higher than the threshold value set via calibrations.

5. Material mapping and the first signs of radiation damage

Using the secondary vertices map for hadronc interactions it is possible to build a nice "hadrography" of the entire detector with a complete material mapping. In figure 11 the plot shows the complete map of the secondary vertices. Zooming at the module level it is possible to find a precise profile of cooling pipes, connectors and even of the decoupling capacitors shown in figure 2.
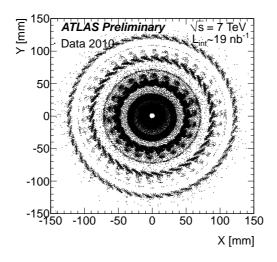

Figure 11: The y vs. x distribution of secondary vertices reconstructed in data. The bin width is 1.5 mm along both axes. All secondary vertices with $|z| < 700$ mm have been used. To aid the eye, only bins with 5 or more entries have been displayed.

9

The Pixel Detector started to show the first signs of radiation damage effects. The integrated luminosity is increasing very rapidly and the expected fluence for the innermost layer, at 50.5 mm from the interaction point, is $\phi \sim 2.4 \cdot 10^{12}$ 1 MeV n$_{eq}$ cm^{-2} per fb^{-1}.

Few different methods are used to monitor the effects of the radiation damage:

- The high voltage leakage current, measured at the power supply channels level, is continuously monitored. The sensitivity of the measurement is 80 nA and, for the time being, six or seven modules, along the beam direction, share the same high voltage channel. Therefore the sensitivity of high voltage current variation per module is at the level of 11 to 13 nA. In future, when the radiation levels will be higher, only one or two modules, due to the leakage current increase and the power supplies capabilities, can be connected to a single high voltage channel, worsening the precision of the measurement.

- In order to keep a sufficiently good resolution on the current measurement that will be worsening in future for the reasons reported in the previous point, it has been decided to install special current monitoring boards for a selected number of channels, placed in different positions both along the beam direction and radially. These specialized current monitoring board have a precision of 10 nA on the measured current and two different gains to monitor lower and higher currents. A number of boards have been already installed for the innermost layer and the complete set will be installed during 2011 and completed by the end of the year.

- The Pixel front-end chip has the capability of measuring the leakage current pixel by pixel. The measurement range and the resolution are optimized for irradiated sensors with a LSB ~ 0.125 nA. Specialized calibration scans are done regularly during LHC technical stops to measure this current. At the time of the conference the radiation effects were not yet enough to have a measurable current via this method, while later in the Summer 2011 the first mesurable effects started to be seen.

- The module depletion voltage is measured with cross-talk scans. A known charge is injected in each pixel while the neighbor pixels are read out. Before type inversion when a module is not fully depleted there are ohmic shorts between pixels and a measurable signal is observed in the neighbor pixels. At increasing voltages the measured signal decreases until reaching a full isolation of pixels from each other. An efficiency S-curve of the number of pixels without hits versus applied voltage allows to determine the depletion voltage, corresponding to the point of derivative sign change on the S-curve. The depletion voltage will decrease until the type inversion and late in Summer 2011 also these effects started to be measurable.

- The depletion depth is constantly monitored using tracks. Before type inversion the measured depth corresponds to the silicon sensor thickness, while after type inversion this method will measure the effective depletion depth without the need of specialized calibration scans.

At the time of the conference the level of radiation was not yet high enough for showing clear results, but soon after, very clear results have been produced with good agreement with the damage models. Based on the results and on a more detailed simulation work done recently, an intense work for more realistic models is ongoing to make precise estimations of the detector lifetime.

6. Pixel Detector status

During these three years of continuous operations we have been calibrating the detector regularly to provide the best possible performance. We have verified that the calibration stability is quite high and that allows to have long period of intense data taking without the need of corrections.

The noise masking is a more frequent and regular operation to achieve the best possible detector conditions. The pixels with a hit rate higher than 10^{-7} hits per pixel per event are masked online in dedicated noise runs. The number of pixels masked is at the level of 0.1 % at the threshold setting of 3500 e. A few additional noisy pixels are masked offline on a run-by-run basis and after this operation the noise rate is as low as 10^{-9} hits per pixel per event corresponding to less than 0.1 noise hits per event for the entire 80 million channels Pixel Detector (fig. 12).
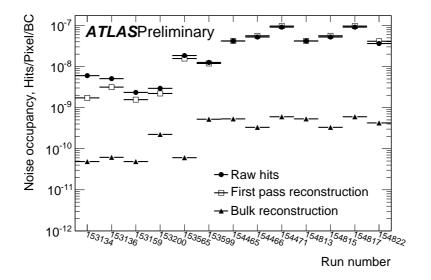

Figure 12: The Pixel Detector occupancy in randomly triggered events with empty bunches. Noise rate is dominated by few pixels (300-1500 out of 80 millions) which are detected on a run-by-run basis by offline prompt calibration and masked during the bulk processing. For the bulk processing, the remaining noise occupancy is $< 10^{-9}$ hits per pixel per event.

In the period between the commissioning in 2008 and the actual data taking we observed failures of few modules. The main source of failures is due to optical communication problems that prevents the configuration of the modules or the correct arrival of data from the modules to the off-detector electronics. Few other failures are due to low voltage shorts and a few others are due to high voltage open lines that prevent to bias the modules. In total the number of disabled modules is 55 out of the total 1744 modules, i.e. 3.2 % of the detector. In addition there are 47 non working front-end chips distributed in the detector. Our current understanding of the failures brings to the conclusion that the detector is sensitive to the temperature oscillations during cooling failures or maintenance. For these reasons the cooling is kept always operational and solutions are being investigated to moderate the temperature gradients in the event of cooling failures. The percentage of failures increased from 2.1 % to the current 3.2 % level during the past three years.
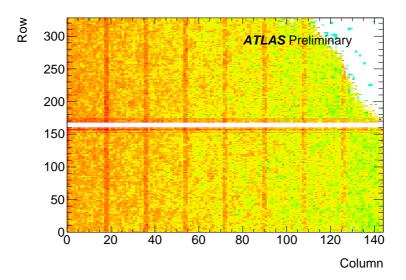
Figure 13: A Pixel Detector module with disconnected bump bonds. The occupancy plot shows a dead region in the upper right part of the module.

The situation with disconnected bump bonds is also monitored constantly and we do not observe an increase with respect to the initial situation. An example of the effect of disconnected bonds on a module can be seen in figure 13 and the overall fraction of these defective pixels in the full detector is a the level of 0.1 %.

At the end of the 2010 proton run, there were unexpected levels of background due to vacuum issues in the warm regions around the LHC Interaction Region 1, where ATLAS is located. The high background caused temporary problems with front-end and back-end buffers, that have been promptly identified and corrected with a new off-detector electronics firmware that can now very efficiently cope with high background situations. The situation of the background in 2011 improved considerably.

7. Conclusions

The Pixel Detector has been operated continuously in the last three years and it is switched on as soon as LHC publishes the "Stable Beams" conditions that allow to safely turn on the most delicate devices as the Pixel Detector.

The Pixel Detector has been participating to the ATLAS data taking periods with an efficiency of 99.5 % or better, where the small percentage below 100 % is mainly due to the switch on time once the "Stable Beams" condition is declared. In a near future a faster automatic switch on procedure will be deployed reducing dramatically the time for this operation.

The time spent during the first phase of the operations to have a very precise calibration has made possible to have a very low dispersion for the threshold settings and a very good charge measurement resolution. The noise occupancy as low as 10^{-9} hits per pixel per event allows the reconstruction of very clearly defined clusters without worrying about noise effects. A number of non-operational modules is now present and solutions to moderate any further increase are being

investigated, as well as possible repair scenarios are being considered for the long LHC shutdown starting at the end of 2012.

The first signs of radiation damage open up a period of intense activity in the future to understand and better model these unavoidable changes of the detector behaviour, while waiting for the insertion of the Insertable B-Layer that will help in keeping the performance of the Pixel Detector on a very high level.

References

[1] G. Aad et al., The ATLAS Experiment at the CERN Large Hadron Collider, JINST 3 (2008) S08003.

[2] G. Aad et al., The ATLAS Pixel Detector electronics and sensors, JINST 3 (2008) P07007.

[3] H. Pernegger, The ATLAS Insertable B-Layer Pixel Detector, Proceedings of this Conference.

[4] I. Peric et al., The FEI3 readout chip for the ATLAS Pixel Detector, Nucl. Instrum. Meth. A 565 (2006) 178; L. Blanquart et al., FE-I2: A Front-End Readout Chip Designed in a Commercial 0.25-μm Process for the ATLAS Pixel Detector at LHC, IEEE Trans. Nucl. Sci., vol. 51, pp. 1358-1364, Aug. 2004.

[5] R. Beccherle et al., MCC: the Module Controller Chip for the ATLAS Pixel Detector, Nucl. Instrum. Meth. A 492 (2002) 117.

[6] C. Jacoboni et al., Solid State Electronics 20 (1977) 77.